# A 25 dBm 95-115 GHz Coupler-Based Traveling-Wave MMIC Power Amplifier in GaAs pHEMT Technology



Citation for the original published paper (version of record):
Kaval, G., Bao, M., Lasser, G. et al (2026). A 25 dBm 95-115 GHz Coupler-Based Traveling-Wave MMIC Power Amplifier in GaAs pHEMT Technology. IEEE MTT-S International Microwave Symposium Digest: 577-580. http://dx.doi.org/10.1109/IMSRFTT43070.2026.11602498

# A 25 dBm 95–115 GHz Coupler-Based Traveling-Wave MMIC Power Amplifier in GaAs pHEMT Technology

Göksu Kaval[#$], Mingquan Bao[&], Gregor Lasser[$], Marcus Gavell[#], Christian Fager[$]
[#]Gotmic AB, Gothenburg, Sweden
[$]Chalmers University of Technology, Gothenburg, Sweden
[&]Ericsson Research, Gothenburg, Sweden
goksu.kaval@gotmic.se

***Abstract*— This paper presents a 95–115 GHz power amplifier (PA) based on a coupler-enabled traveling-wave combiner/splitter network, implemented in a commercial 0.1 µm GaAs pHEMT process. Directional couplers provide high inter-branch isolation, suppressing mutual load interactions between the combined unit amplifiers. The PA achieves a saturated output power of 24.5 dBm (±0.7 dB) across a 20 GHz bandwidth, representing one of the highest reported power levels for GaAs PAs beyond 100 GHz. These results demonstrate the effectiveness of the coupler-based traveling-wave architecture for wideband, high-power W-band MMIC design.**

***Keywords*— Gallium Arsenide (GaAs), MMIC, power amplifier (PA), power combining, traveling-wave amplifier (TWA), W-band.**

## I. Introduction

High-resolution radar systems and high-data-rate wireless links both benefit from the wide contiguous spectrum available in the W-band. Demonstrations have been reported in [1] for radar and up to 114 GHz in [2] for telecommunications.

To realize these systems, power amplifiers (PAs) are critical for generating the required transmit power. Gallium Arsenide (GaAs) HEMT technology remains a cost-effective and mature solution for such PAs, particularly for applications beyond 100 GHz [3]. However, its lower power density compared to GaN necessitates large-periphery devices with low optimum load impedances, creating a severe power-bandwidth trade-off due to high impedance transformation ratios [4]. Consequently, power combining multiple individually matched unit amplifiers (UAs) is the preferred approach for achieving high output power over a wide bandwidth.

Non-uniform distributed power amplifiers (NDPAs) can be employed for this purpose, with successful implementations reported recently in GaN for V-/E-band [5] and in GaAs for E-band [6]. However, a significant drawback of this topology is that the load impedance presented to each UA is dependent on the power contribution of other branches, leading to load-pull interactions. As reviewed in [7], NDPA structures often exhibit reduced output power and power added efficiency (PAE) compared to the intrinsic device capability. To address this, a traveling-wave amplifier (TWA) with inter-branch isolation was demonstrated for W-band GaN applications in [8], [9]. This topology, rooted in the divider concepts of [10] and first adapted for MMIC PAs in [11], effectively decouples the power combining and impedance matching functions.

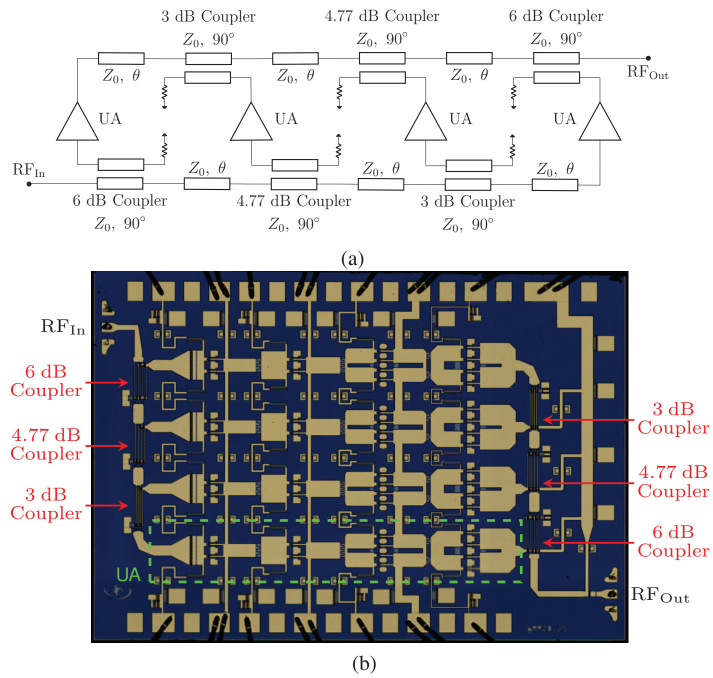


Fig. 1. (a) Circuit diagram of the TWA with inter-branch isolation. (b) Chip photo of the fabricated MMIC PA ($3.1 \times 2.1$ mm) with simplified functional blocks annotated.

In this work, we present a TWA with inter-branch isolation shown in Fig. 1 implemented in a commercial 0.1 µm GaAs pHEMT process (WIN PP10-20). By adopting this topology, we achieve a saturated output power of up to 25.2 dBm, demonstrating the potential of this approach for high-performance W-band GaAs MMICs.

## II. Design Concept

The design consists of four UAs (Fig. 2) power-combined using a traveling-wave architecture utilizing directional couplers, as illustrated in Fig. 1a. The input distribution network employs a series of Lange couplers with a characteristic impedance of $Z_0$. The coupling coefficients in this network are tapered to ensure that a specific fraction of the input power is coupled to each branch, resulting in a uniform drive level for all UAs. Similarly, the output network utilizes a complementary arrangement of couplers to coherently combine the amplified signals into the main transmission line.

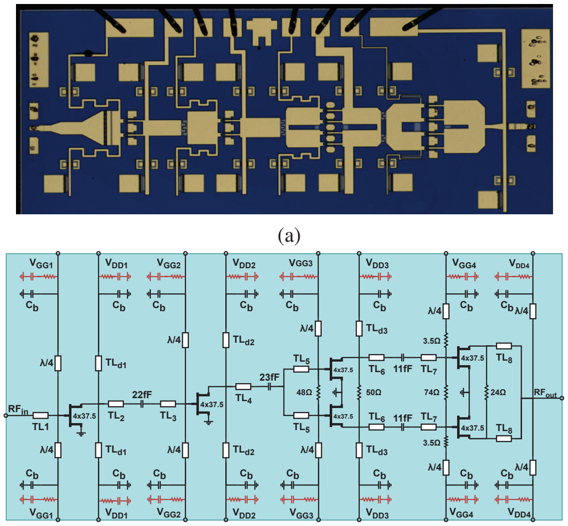

(a)

(b)

Fig. 2. (a) Layout and (b) circuit diagram of the manufactured UA cell (2.6 × 1.0 mm).

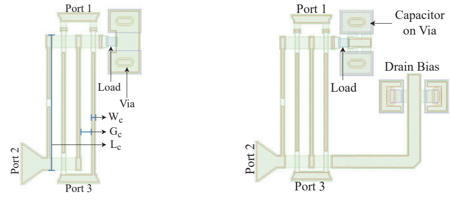

(a) (b)

Fig. 3. Layout of the Lange couplers. (a) Input coupler structure. (b) Output coupler illustrating the DC bias injection through the Lange fingers.

Table 1. Physical and Simulated Parameters of Designed Couplers

| Parameter | Coupler 1 | Coupler 2 | Coupler 3 |
|---|---|---|---|
| Gap ($G_c$) ($\mu$m) | 5.2 | 11.7 | 17.0 |
| Width ($W_c$) ($\mu$m) | 8.0 | 8.0 | 7.0 |
| Length ($L_c$) ($\mu$m) | 240 | 230 | 220 |
| Coupling (dB) | 3.3 | 5.1 | 6.3 |
| $\lvert Z_c \rvert$ ($\Omega$) | 36 | 37 | 38 |
| Directivity (dB) | 16.9 | 17.5 | 17.6 |
| Dissipation Loss (dB) | 0.14 | 0.13 | 0.13 |

Additionally, interconnecting transmission lines with electrical length $\theta$ are incorporated to accommodate UAs of arbitrary physical size. In this arrangement, RF power amplitude variances between UAs—caused by non-idealities such as self-biasing or thermal gradients—do not affect the impedance presented to other UAs due to the high inter-port isolation. Furthermore, the coupler topology inherently improves the input and output matching.

## III. Circuit Implementation

The circuit was fabricated in the WIN Semiconductors PP10-20 pHEMT process, featuring 0.1 µm D-mode transistors ($f_T = 160$ GHz) and two metal layers. Simulations were performed in Keysight ADS using foundry active models and calibrated EM passive structures.

The couplers in the combiner/splitter topology in Fig. 1a are realized as the Lange couplers shown in Fig. 3. The couplers were designed to have a characteristic impedance ($Z_c$) of 36 Ω, as standard 50 Ω designs would require unfeasibly thin fingers in this process. This establishes the system impedance of the combiner/splitter network as $Z_0 = Z_c = 36\,\Omega$. In the output combiner, the drain bias is injected into the UAs through the Lange coupler fingers without degrading their performance. Consequently, the standard shorting vias of the terminated port are replaced with bypass capacitors to provide an RF ground while maintaining DC isolation, as shown in Fig. 3b. Table 1 summarizes the physical dimensions and simulated metrics, including coupling ($-|S_{23}|_{\mathrm{dB}}$), directivity ($|S_{32}|_{\mathrm{dB}} - |S_{12}|_{\mathrm{dB}}$), and dissipation loss ($-10\log_{10}(|S_{13}|^2 + |S_{23}|^2 + |S_{33}|^2)$). The characteristic impedance of couplers is defined as $Z_c = \sqrt{Z_{\mathrm{odd}} Z_{\mathrm{even}}}$. The isolation load was replaced by Port 4 strictly for odd-even impedance analysis, whereas other parameters were characterized with the termination resistor [12].

The UAs consist of four common-source stages. The first two stages employ two $2 \times 37.5\,\mu$m transistors sharing a common source via. The third and fourth stages utilize four $2 \times 37.5\,\mu$m transistors, also employing a shared via configuration. When biased at 4 V with a current density of 300 mA/mm, a single $2 \times 37.5\,\mu$m device provides a Maximum Available Gain (MAG) of 7.1 dB and 6.1 dB at 100 GHz and 114 GHz, respectively. The output power at 1 dB compression ($P_{1\mathrm{dB}}$) at these frequencies is 15.4 dBm and 15.7 dBm, respectively. At the center frequency of 107 GHz, the source ($Z_S$) and load ($Z_L$) impedances required for a simultaneous conjugate match are $Z_S = (5.0 - j9.9)\,\Omega$ and $Z_L = (8.7 + j13.5)\,\Omega$.

Simulations revealed that the optimal impedances for simultaneous conjugate matching, saturated output power, and peak PAE are nearly coincident. Consequently, all stages were conjugately matched. To interface properly with the power combiner, the input and output ports of the UA were matched to 36 Ω. The implementation of these matching networks is shown in Fig. 2b, with transmission line parameters listed in Table 2. A key layout constraint was the realization of the drain bias feeds ($\mathrm{TL}_{dn}$), which required wide traces to handle the high current density. Because these wide lines offer limited routing flexibility, their lengths were fixed, and the matching networks were optimized to absorb and compensate for their parasitic electrical response.

Table 2. RF Parameters of Transmission Lines

| TL | $Z_c$ (Ω) | Length (°) | TL | $Z_c$ (Ω) | Length (°) |
|---|---|---|---|---|---|
| $\mathrm{TL}_1$ | 20 | 35 | $\mathrm{TL}_7$ | 28 | 70 |
| $\mathrm{TL}_2$ | 32 | 75 | $\mathrm{TL}_8$ | 24 | 83 |
| $\mathrm{TL}_3$ | 20 | 65 | $\mathrm{TL}_{d1}$ | 57 | 52 |
| $\mathrm{TL}_4$ | 28 | 84 | $\mathrm{TL}_{d2}$ | 58 | 49 |
| $\mathrm{TL}_5$ | 30 | 66 | $\mathrm{TL}_{d3}$ | 42 | 32 |
| $\mathrm{TL}_6$ | 31 | 78 | | | |

Stability analysis for the amplifiers was conducted by first verifying that individual transistors are unconditionally stable at the operating frequency. Subsequently, the absence of right-half-plane poles was confirmed at every circuit interface using Nyquist contours. The analysis necessitated

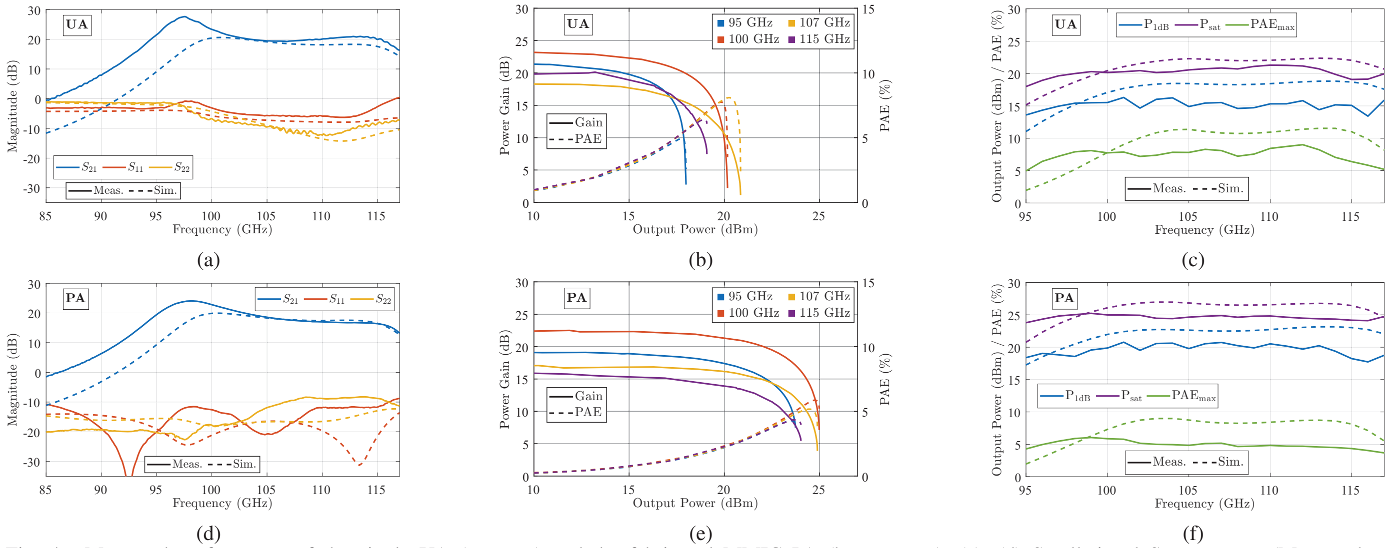


Fig. 4. Measured performance of the single UA (top row) and the fabricated MMIC PA (bottom row). (a), (d) Small-signal S-parameters (Measured vs. Simulated). (b), (e) Measured Power Gain and PAE versus Output Power at selected frequencies. (c), (f) Large-signal performance summary ($P_{\mathrm{sat}}$, $P_{\mathrm{1dB}}$, and Peak PAE) versus frequency.

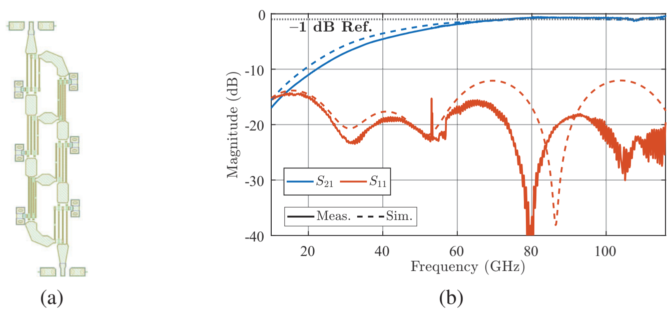


Fig. 5. Back-to-back combiner test structure (a) and measured S-parameters (b).

the placement of a 3.5 Ω series resistor at the gate bias terminal as shown in Fig. 2a. Additionally, resistors with values of 48 Ω, 50 Ω, 74 Ω, and 24 Ω indicated in Fig. 2a were placed between transistors across the even symmetry plane to suppress odd-mode oscillations. Furthermore, when combining the UAs, additional series resistors of 2.5 Ω were incorporated into the gate bias networks to enhance the stability margin. Finally, on-chip decoupling networks, implemented as shunt RC combinations of a 7 Ω resistor and a 5 pF capacitor, were included as highlighted in red in Fig. 2b.

## IV. Measurement Results and Discussion

The MMIC PAs were mounted on a test PCB. The bias pads were wire-bonded directly to an adjacent 120 pF single-layer capacitor, followed by parallel 100 nF and 1 µF surface-mount capacitors on the PCB. The RF ports were contacted using 1.0 mm coaxial probes. Small-signal measurements were performed using a vector network analyzer (VNA) equipped with frequency extenders, calibrated using on-wafer Line-Reflect-Match (LRM) standards. For large-signal characterization, a driver amplifier was inserted at the input to drive the PA into saturation. At the output, a 20 dB attenuator and a directional coupler were connected in cascade after a WR-10 waveguide probe. The gain, normalized to a through calibration, was monitored by the VNA via the coupled port, while an Erickson PM5 power meter connected to the through port of the coupler measured the absolute output power.

The small-signal measurements of the UA (Fig. 4a) and the PA (Fig. 4d) show good agreement with simulations, particularly regarding the gain response. However, the UA exhibits an input reflection coefficient ($|S_{11}|$) in close proximity to 0 dB, which indicates that the amplifier is marginally stable. In contrast, the PA exhibits significantly improved return loss at both the input and output ports, attributed to the use of directional couplers.

The back-to-back test structure of the combiner is shown in Fig. 5a, with the corresponding measurements presented in Fig. 5b. The measured back-to-back insertion loss remains below 1 dB across the operating frequency range, implying an insertion loss of less than 0.5 dB for a single power combiner. The close agreement between the simulated and measured responses validates the accuracy of the EM models used for the passive structures.

The dynamic gain and PAE of the UA (Fig. 4b) and the PA (Fig. 4e) demonstrate that the combiner successfully increases the saturated output power by approximately 5 dB. While an ideal four-branch combination yields a 6 dB increase, the back-to-back measurements in Fig. 5b reveal a 0.5 dB insertion loss attributed to the combiner itself. The remaining discrepancy likely stems from non-idealities, such as phase imbalance due to device process spread or thermal coupling effects.

Finally, the output power at 1 dB compression ($P_{\mathrm{1dB}}$), saturated output power ($P_{\mathrm{sat}}$), and peak PAE ($\mathrm{PAE}_{\mathrm{max}}$) are presented for the UA (Fig. 4c) and the PA (Fig. 4f).

Measurements reveal a deviation of approximately 2 dB between the measured and simulated output power in both designs, indicating that the performance degradation originates within the unit amplifier rather than the combining network. Furthermore, the significant difference between $P_{\mathrm{1dB}}$ and $P_{\mathrm{sat}}$ suggests soft compression characteristics. This observation, combined with the measured drain currents, confirms that the driver stages saturate prematurely, before the output stage reaches full compression. Consequently, future designs would benefit from reducing the inter-stage periphery ratio (especially between stages 2 and 3) to achieve simultaneous saturation. Notwithstanding this, the design delivers a saturated output power of 24.5 dBm (±0.7 dB) from 95 to 115 GHz with over 16.4 dB of gain. This 20 GHz bandwidth is particularly notable for GaAs works given the high impedance transformation ratio required to match the optimal load of the UA output stage ($Z_{\mathrm{L}} = 2.2 + j3.3\,\Omega$) to the combiner impedance.

Table 3. Comparison with State-of-the-Art W-Band Amplifiers

| Work | Process | Freq. (GHz) | Gain (dB) | $P_{\mathrm{sat}}$ (dBm) | PAE (%) | P.D. (mW/mm$^2$) |
|---|---|---|---|---|---|---|
| [13] | GaN | 102–118 | 16.9–21.4 | 27.4–29.1 | 8 | 124.1 |
| [14] | GaAs | 100–113 | 3.0–6.7 | 20.3–24.0 | - | 48.3 |
| [15] | GaAs | 85–116 | 15.0–25.0 | 20.0–25.0 | 4 | 38.3 |
| [16] | GaAs | 100–114 | 15.2–18.2 | 19.3–24.1 | 11.9 | 41.2 |
| **T.W.** | **GaAs** | **95–115** | **16.4–24.0** | **23.8–25.2** | **5.8** | **50.9** |

P.D.: MMIC Power Density; T.W.: This Work

Table 3 summarizes the gain, $P_{\mathrm{sat}}$, and $\mathrm{PAE}_{\mathrm{max}}$ achieved by the fabricated PA within the operating frequency band, alongside state-of-the-art amplifiers. Compared to recent GaAs implementations [15], [16], this work demonstrates superior output power—with a flatness of ±0.7 dB—and power density, while maintaining a competitive operating bandwidth. Although GaN technologies [13] inherently support higher power densities, these results confirm that the coupler-based topology effectively minimizes implementation losses, enabling the MMIC to approach the intrinsic saturated power limit of the GaAs pHEMT process across a wide bandwidth.

## V. Conclusion

A coupler-based traveling-wave amplifier operating from 95 GHz to 115 GHz has been demonstrated. Implemented in a commercial 0.1 µm GaAs pHEMT technology, the architecture leverages the high isolation of directional couplers to separate the power-combining function from impedance-matching constraints. This approach mitigates the mutual load interactions typical of conventional distributed amplifiers, allowing each UA to operate near its optimal large-signal load line. Measurements show a saturated output power of 24.5 dBm (±0.7 dB) across a 20 GHz bandwidth. By providing high isolation between the UAs, the architecture ensures that the combined PA closely tracks the standalone UA's power capabilities with minimal combining penalty.

## Acknowledgment

The authors gratefully acknowledge WIN Semiconductors for providing access to their PP10-20 process as part of the WIN University Multi-Project Wafer Program. This project has received funding from the Eurostars 3 programme with co-funding from the European Union's Horizon Europe research and innovation programme. The authors also thank Mathias Huggert for manufacturing the test PCBs for the presented circuits.

## References

[1] B. Welp, S. Hansen, G. Briese, S. Küppers, S. Thomas, C. Bredendiek, and N. Pohl, "Versatile dual-receiver 94-GHz FMCW radar system with high output power and 26-GHz tuning range for high distance applications," *IEEE Trans. Microw. Theory Techn.*, vol. 68, no. 3, pp. 1195–1211, 2020.

[2] M. Hörberg, B. Madeberg, D. Sjöberg, H. Zirath, K. Bitsikas, K. Kravariotis, S. Tsapalis, M. Gavell, G. Granström, R. Lövblom, D. Siomos, S. Agneessens, and J. Hansryd, "A W-band, 92–114 GHz, real-time spectral efficient radio link demonstrating 10 Gbps peak rate in field trial," in *Proc. IEEE/MTT-S Int. Microw. Symp. (IMS)*, 2022, pp. 545–548.

[3] V. Camarchia, R. Quaglia, A. Piacibello, D. P. Nguyen, H. Wang, and A.-V. Pham, "A review of technologies and design techniques of Millimeter-wave power amplifiers," *IEEE Trans. Microw. Theory Techn.*, vol. 68, no. 7, pp. 2957–2983, 2020.

[4] R. Fano, "Theoretical limitations on the broadband matching of arbitrary impedances," *Journal of the Franklin Institute*, vol. 249, no. 1, pp. 57–83, 1950.

[5] C. Bharath, M. Bao, C. Friesicke, S. Wagner, and R. Quay, "A 52-to-86GHz V-/E-band GaN distributed combined power amplifier with output power beyond 1 W and 34GHz bandwidth," in *Proc. IEEE/MTT-S Int. Microw. Symp. (IMS)*, 2024, pp. 850–853.

[6] Z. Li, Q. Yu, and J. Zhang, "E-band power amplifier with 32.2 dBm $\mathrm{P_{sat}}$, 31.3 dBm $\mathrm{OP_{1dB}}$ utilizing commercial 0.10-mm GaAs pHEMT technology," in *Proc. IEEE/MTT-S Int. Microw. Symp. (IMS)*, 2025, pp. 729–732.

[7] C. F. Campbell, "Evolution of the nonuniform distributed power amplifier: A distinguished microwave lecture," *IEEE Microw. Mag.*, vol. 17, no. 6, pp. 18–28, June 2016.

[8] J. M. Schellenberg, "A 2-W W-band GaN traveling-wave amplifier with 25-GHz bandwidth," *IEEE Trans. Microw. Theory Techn.*, vol. 63, no. 9, pp. 2833–2840, 2015.

[9] S. Verploegh, M. Pinto, L. Marzall, D. Martin, G. Lasser, and Z. Popović, "Analysis of process variations in W-band GaN MMIC PAs using nonparametric statistics," *IEEE Transactions on Microwave Theory and Techniques*, vol. 69, no. 4, pp. 2304–2318, 2021.

[10] R. Mohr, "A microwave power divider (correspondence)," *IRE Trans. Microw. Theory Techn.*, vol. 9, no. 6, pp. 573–573, 1961.

[11] M. Knox, R. Youmans, M. Kumar, L. Forker, H. Voigt, P. Brand, F. Marcotte, and A. Hughes, "400 W X-band GaAs MMIC CW amplifier," in *Proc. IEEE MTT-S Int. Microw. Symp.*, 1995, pp. 1605–1608 vol.3.

[12] P. Toulios and A. Todd, "Synthesis of symmetrical TEM-mode directional couplers," *IEEE Trans. Microw. Theory Techn.*, vol. 13, no. 5, pp. 536–544, 1965.

[13] E. Camargo, J. Schellenberg, L. Bui, and N. Estella, "F-band, GaN power amplifiers," in *Proc. IEEE/MTT-S Int. Microw. Symp. (IMS)*, 2018, pp. 753–756.

[14] H. Wang, L. Samoska, T. Gaier, A. Peralta, H. H. Liao, Y. C. Chen, M. Nishimoto, and R. Lai, "Monolithic power amplifiers covering 70–113 GHz," in *Proc. IEEE Radio Freq. Integr. Circuits (RFIC) Symp.*, 2000, pp. 39–42.

[15] S. J. Mahon, J. Mihaljevic, S. Chakraborty, M. C. Gorman, M. C. Heimlich, and Y. Li, "Microstrip GaAs power amplifiers for high capacity 92–114 GHz 5G and 6G backhaul," in *Proc. Eur. Microw. Integr. Circuits Conf. (EuMIC)*, 2022, pp. 157–160.

[16] G. Kaval, G. Lasser, M. Gavell, and C. Fager, "A balanced 100–114-GHz Millimeter-wave GaAs MMIC power amplifier with high gain," *IEEE Microw. Wireless Technol. Lett.*, pp. 1–4, 2025.